Progress of Theoretical Physics, Vol. 74, No. 5, November 1985

Spatiotemporal Intermittency in Coupled Map Lattices

Kunihiko KANEKO

Institute of Physics, College of Arts and Sciences
University of Tokyo, Tokyo 153

(Received June 17, 1985)

Spatiotemporal intermittency is investigated in a class of coupled map lattices. Burst and laminar regions form a geometrical structure in spacetime, which is analogous to the ones found in cellular automata. Mechanism of the formation of this structure is discussed, with the study on the critical properties of the propagation speed of bursts and distribution of laminar clusters. Lyapunov spectra are calculated, which show the existence of two kinds of motions, i.e., laminar and bursts. Possibility of a "mean field theory" for coupled chaos is also discussed.

§ 1. Introduction

Theories for low-dimensional dynamical systems have made a great success for the description of the onset of turbulence and the statistical properties for the weak turbulence.[1] The studies of chaos have formed a new paradigm to understand the system where the nonlinearities are essential. Fluid turbulence has been a cradle for the development of the new paradigm, but it has not yet been clear whether the developed turbulence can be understood from the viewpoint of chaos.

One fascinating idea for the turbulence is to regard it as a direct product state of elementary low-dimensional systems. Landau took a limit cycle as the elementary system and considered a model for the turbulence as a quasiperiodic state with infinite number of incommensurate frequencies,[2] which has been denied by Ruelle and Takens' picture[3] and by the abundance of lockings.[4]

Then, what happens if we choose a low-dimensional chaos as an elementary system? This question has led the author to construct and study the "coupled map lattice" model, which is given by

$$x_{n+1}(i)=f(x_n(i))+\frac{\epsilon}{2}\{g(x_n(i+1))+g(x_n(i-1))-2g(x_n(i))\}$$

$(i=1, 2, \cdots, N)$ with periodic boundary condition.

In the previous papers,[5] the following aspects were found for the "coupled logistic lattice", i.e., $f(x)=1-Ax^2$ and $g(x)=x$ or $g(x)=f(x)$: (i) Period-doubling of kink-antikink patterns: Spatial complexity is increased by the doublings and the number of possible attractors also increase rapidly, each of which is characterized by the number and the position of kinks. (ii) Zigzag patterns (or antiferro-like structures): A zigzag structure with a wavelength-two appears, which again have some kinks. This type of structure is stable not only for a cycle with period-two but also for a quasiperiodic or chaotic state. (iii) Spatiotemporal intermittency: Burst and laminar regions form complicated spatiotemporal patterns at some values of coupling ϵ. For larger couplings, burst regions dominate, while they disappear for smaller couplings.

Recent studies for coupled map lattices have also revealed a new type of intermittency

in strong coupling regimes,[6] two-dimensional zigzag patterns,[7] period-doublings in open flow,[8] and condensation of chaos gases[9] and so on.[10)~13)]

In the present paper, we investigate the spatiotemporal intermittency in more detail. The motivations for the study are as follows: (a) "Intermittency has been used in two different meanings, i.e., one for the intermittency by Pomeau and Manneville[14] where the notion is purely temporal in low-dimensional dynamical systems and the other for the original meaning in fluid mechanics where the spatiotemporally self-similar structures of eddies are essential.[15] It has not yet been clear, however, whether the above two notions are related or not. Though our model cannot establish the relationship, it might give a step towards the understanding of it, in the sense that our model starts from Pomeau and Manneville's intermittency and shows spatiotemporally geometrical structures. (b) A reduction to finite states (burst or laminar) is useful, which shows clearly the geometrical strucure in spacetime. The pattern thus obtained looks quite like the ones in cellular automata recently found by Wolfram.[16] Spatiotemporal intermittency of our model gives an example to connect a coupled map lattice with a cellular automaton, which may be useful for the future study in nonlinear physics. (c) As the coupling is increased, the numbers of positive Lyapunov exponents increase and a kind of "fully developed turbulence" appears, where we can check whether the motion can be regarded as a direct product state of elementary one-dimensional chaos.

The construction of this paper is as follows: In § 2, three coupled map lattices are introduced for the study of spatiotemporal intermittency. Phase transition from laminar states to burst states is explained in § 3. Section 4 is devoted to visualization of spatiotemporal patterns, where a reduction to two states is used. In § 5, an approach to understand the pattern is shown, though, the complete understanding of the mechanism for the pattern is left to future. Numerical results for the Lyapunov spectra are shown in § 6. Discussions are given in § 7.

§ 2. Models

As models for the spatiotemporal intermittency, we consider the case where the one-dimensional map $x_{n+1}=f(x_n)$ shows a stable periodic cycle but the stability is weak and Pomeau and Manneville's intermittency[14] occurs at the nearby parameters. The models we studied numerically are as follows:

(A)
$$f(x)=\begin{cases} x+x^2+a, & (x<c) \\ -3(x-c)+1+a, & (x>c) \end{cases}$$
$$c\equiv(\sqrt{5}-1)/2;\quad g(x)=f(x)\,,$$

where a is a small negative parameter. In this case, a stable fixed point exists at $x=x^*=-\sqrt{-a}$ for the one-dimensional map $x_{n+1}=f(x_n)$ (see Fig. 1(a)). The region $x\sim x^*$ corresponds to the laminar region.

(B) Coupled Circle Lattice
$$f(x)=x+A\sin 2\pi x+C\,,\quad (\mathrm{mod}\ 1)$$
$$g(x)=\sin 2\pi x\,,$$

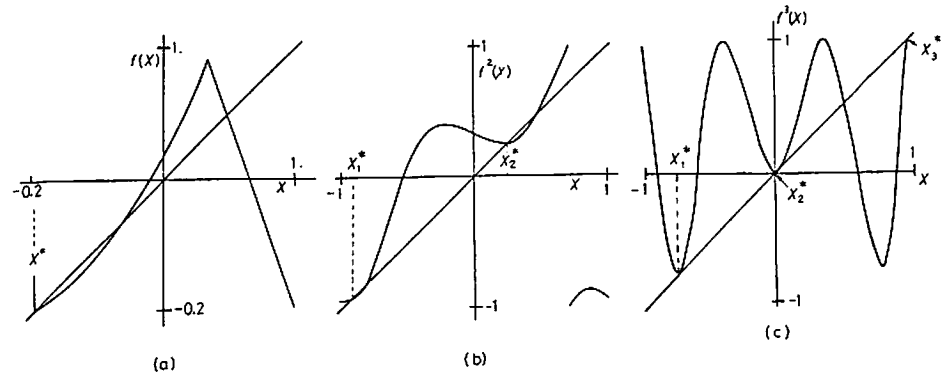

Fig. 1. (a) One-dimensional map $x_{n+1}=f(x_n)$ for model (A) with $a=-0.05$.
(b) Twice-iterated circle map $x_{n+1}=f^2(x_n)$ ((B)) with $A=0.2$ and $C=0.55$.
(c) Three-times iterated logistic map $x_{n+1}=f^3(x_n)$ ((C)) with $A=1.752$.

where $A=0.2$ and $C=0.55$, at which a stable cycle with period two ($x_2^*=f(x_1^*)$, $x_1^*=f(x_2^*)$) exists for the one-dimensional map (see Fig. 1 (b)).

(C) Coupled Logistic Lattice
$$f(x)=1-Ax^2\,,$$
$$g(x)=f(x)\,,$$

where A is chosen to be 1.752, which is slightly larger than the onset value for the appearance of a stable three-cycle via the intermittent transition ($x_2^*=f(x_1^*)$, $x_3^*=f(x_2^*)$ and $x_1^*=f(x_3^*)$ (see Fig. 1 (c)).

In these models, the one-dimensional maps $x_{n+1}=f(x_n)$ are chosen so that the intermittent transition by Pomeau and Manneville[14] occurs if the parameters (a, A or C and A respectively) are changed slightly. We note that the topological chaos exists in the dynamics $x_{n+1}=f(x_n)$ for these models and the chaotic orbit appears as a transient before the orbit is attracted into the stable cycle. The existence of topological chaos seems to be essential for the spatiotemporal intermittency in a coupled system. The features to be described in later sections do not change if the parameters are slightly changed for these models or if the coupling $g(x)$ takes a different form.

§ 3. Phases

There occurs a phase change for the attractor as the coupling is increased, if the initial condition is not a trivial one (e.g., $x(i)=$constant is a trivial one). For a very small coupling the pattern is essentially the same as in the case without coupling. Thus, the attractor is cycle (with period one for model (A), two for (B), and three for (C)), though the phases of the cycles can differ sites by sites for the last two models. For a larger coupling the attractor is chaotic, where bursts exist spatiotemporally.

The bursts are characterized as follows: First, the value $x(i)$ deviates largely from the values of the stable periodic points for the one-dimensional map; second, the time

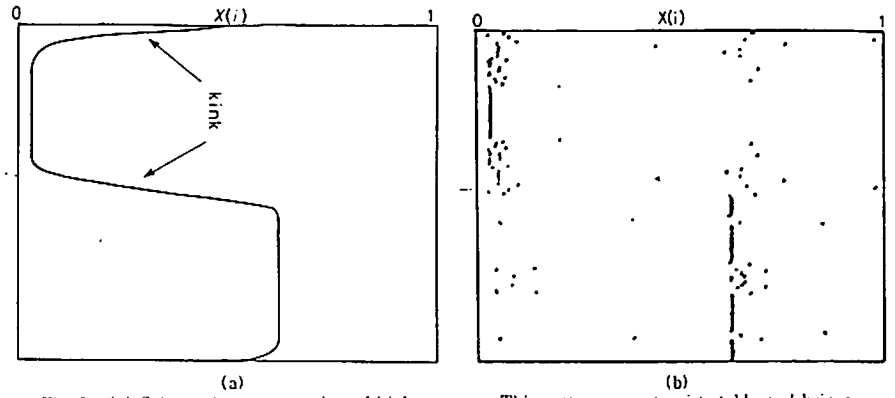

Fig. 2. (a) Schematic representation of kink pattern. This pattern cannot exist stably and brings about the pattern in (b).
(b) Snapshot for $x_n(i)$ for model (B) with $\varepsilon=0.024$ from the initial condition $x_0(i)=\sin(2\pi i/N)$, after the transients have decayed out.

series of $x(i)$ show a chaotic behavior; third, the difference between the values $x(i)$ for the neighboring sites does not remain small.

The third aspect is due to the existence of topological chaos for the one-dimensional map $x_{n+1}=f(x_n)$, i.e., the map $x_{n+1}=f(x_n)$ shows the sensitive dependence on the initial condition in some regions of x, where x is not close to the periodic points x_i^*.

To make the third point clear, we consider the initial condition $x(i)=x_1^*$ $(1<i\leq N/2)$ and $x(i)=x_2^*(N/2<i\leq N)$ for models (B) and (C). When the nonlinearity in one-dimensional map $x_{n+1}=f(x_n)$ is small and there is no topological chaos, a kink-antikink pattern stably exists, which is schematically shown in Fig. 2(a). A typical example of such patterns is the period-doubling of kink-antikinks studied in the previous papers.[5]

In our case, this pattern cannot stably exist, because in the region of a kink or antikink, $x_n(i)$ can take the value at which the one-dimensional map $x_{n+1}=f(x_n)$ shows a transient chaotic behavior. Thus, the kinks or antikinks become bursts which propagate if the coupling is large enough. For example, see Fig. 2(b) for the snapshot of model (B).

The "phase transition" from a direct product state to a burst state is not simple at all in the parameter space. We note the following aspects:

(i) The transition occurs not at one point in the parameter space but at many points. That is, for $\varepsilon>\varepsilon_0$ we have a burst state, and for $\varepsilon_0>\varepsilon>\varepsilon_1$ we have a laminar state, and for $\varepsilon_1>\varepsilon>\varepsilon_2$ again a burst state, and so on. As we study in more detail in the parameter space, there appears more transition points. See, for example, Fig. 3 for the phase diagram for model (A). The structure here was found in the parameter space for a fixed initial condition, though this type of fine structure was also observed in basin structures,[17),18)] and in the velocity space of colliding kinks in a ϕ^4 system.[19)]

(ii) Near the transition region, we have observed some complicated phases for models (B) and (C). Examples are as follows:

a) Kinks and antikinks are recombined and a homogeneous phase appears.

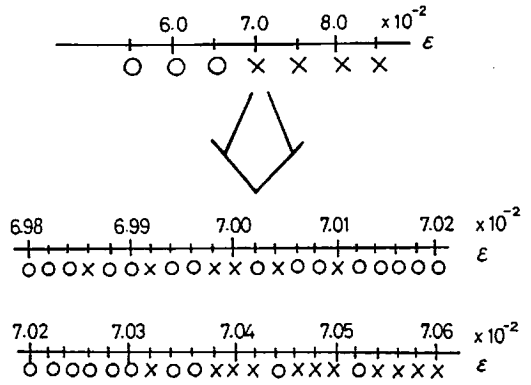

Fig. 3. Phases for model (A) with the initial condition $x_n(50)=0.01$ and $x_n(i)=x^*$ for $i\neq 50$. $N=100$ and $a=-0.01$. ○ denotes the laminar phase (i.e., $x_n(i)=x^*$ for all i), while × denotes the burst phase.

b) Localized chaos; the burst regions exist but they cannot propagate into the whole space and are confined within some regions. Examples are shown in the next section.

§ 4. Visualization
— *Cellular automaton reductions* —

Here we give some pictures for the patterns of bursts and laminar clusters. Patterns in model (B) are shown in Fig. 4, where initial conditions are chosen to be $x(i)=x_1^*$ (for $1<i\leq N/2$) and $x(i)=x_2^*(N/2<i\leq N)$. That is, bursts exist initially only at sites $i=N$ and $i=N/2$. Here, the following reduction method to two-state cellular automata is used; $S(i)=1$ if $|x(i+1)-x(i)|\pmod 1>\delta$ $(\delta=0.05)$ and $S(i)=0$ otherwise. In the figures, the sites with $S(i)=1$ are shown by dots. Figure 5 gives the pattern for the same model with the same reduction, but with the initial condition $x(i)=$random number homogeneously distributed in (0, 1).

Some patterns for model (C) are shown in Fig. 6, where initial conditions are again random or $x(i)=x_1^*$ (for $1<i\leq N/2$) and $x(i)=x_2^*$ (for $N/2<i\leq N$) and the criterion for the burst is given by $|x(i+1)-x(i)|>0.1$.

We note the following aspects:

(1) The geometrical pattern of burst and laminar states: Clusters of laminar sites with various sizes form a structure with a similarity, which is quite analogous to the patterns in cellular automata found by Wolfram.[16)] The difference between coupled map lattices and cellular automata lies in the complexity of an element itself in the former models. Since some stochastic aspects must be taken into account by the coarse graining, it is rather astonishing that the reduction to two-state cellular automata works rather well for the present case.

(2) Localized chaos: As has been described in § 3, the burst remains in a limited space for some parameter regions. Here we note that the pattern looks quite similar to the growth

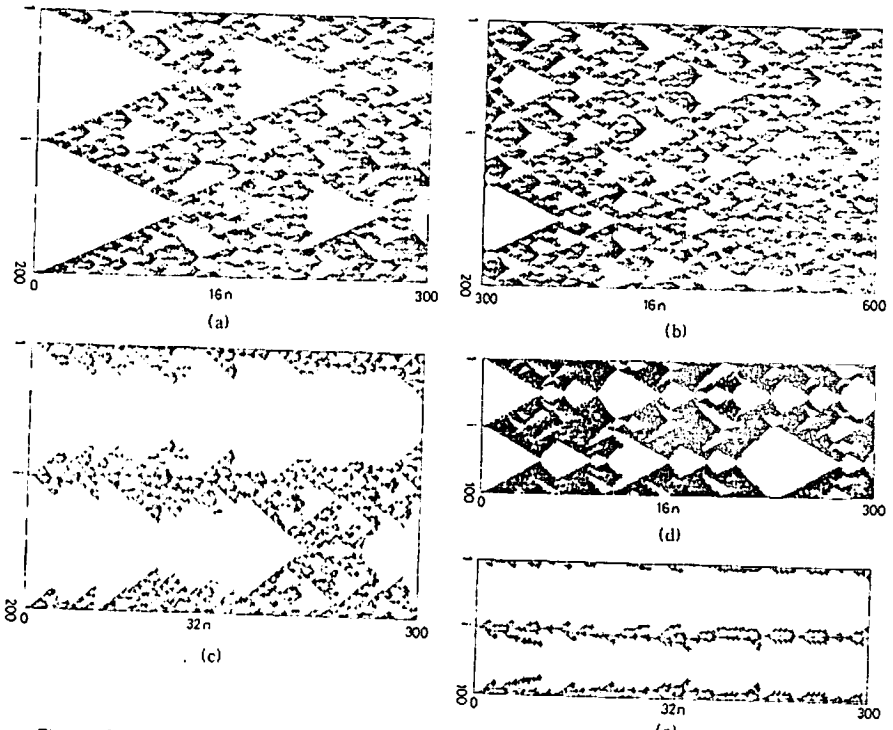

Fig. 4. Spatiotemporal patterns for model (B) with the initial condition $x(i)=x_1^*$ (for $1<i\leq N/2$) and $x(i)=x_2^*$ (for $N/2<i\leq N$). See the text for the method of visualization.
(a) $N=200$ and $\varepsilon=0.024$. $x_{16n}(i)$'s are plotted for $0<n<300$.
(b) Continued from (a). $x_{16n}(i)$'s are plotted for $300<n<600$.
(c) $N=200$ and $\varepsilon=0.0238$. $x_{32n}(i)$'s are plotted for $0<n<300$.
(d) $N=100$ and $\varepsilon=0.025$. $x_{16n}(i)$'s are plotted for $0<n<300$.
(e) $N=100$ and $\varepsilon=0.0236$. $x_{32n}(i)$'s are plotted for $0<n<300$.

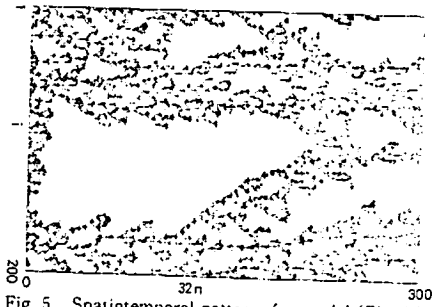

Fig. 5. Spatiotemporal patterns for model (B) with the random initial condition, i.e., $x(i)$ =homogeneous random number in (0, 1). $x_{32n}(i)$'s are plotted for $0<n<300$ with the use of the same method as in Fig. 4 for visualization.

of dendritic crystals.

(3) Self-organization from random initial configurations: The simulations from the random initial configuration give similar figures to the corresponding patterns in Fig. 4. That is, the geometrical structure or dendritic-crystal-like pattern appears also from random initial configurations. Thus, these patterns are inherent to our dynamical system, not due to the special choice of the initial condition.

(4) The patterns in model (C) are not so beautiful as those for model (B), in the sense that the geometrical pattern with self-similarity cannot be clearly seen. In

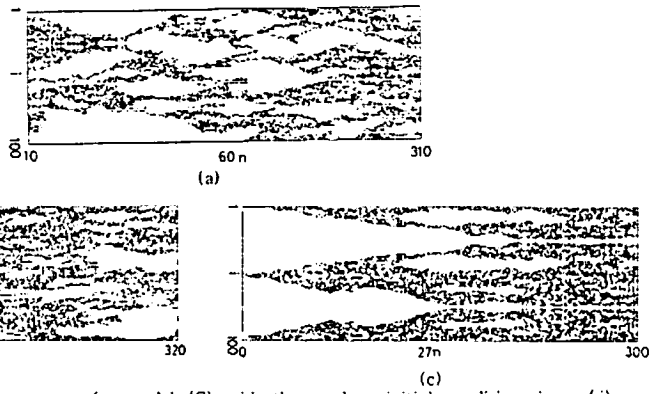

Fig. 6. Spatiotemporal patterns for model (C) with the random initial condition, i.e., $x(i)$ =homogeneous random number in (0, 1) for (a) and (b) and with the initial condition $x(i)=x_1^*$ (for $1<i\leq N/2$) and $x(i)=x_2^*$ (for $N/2<i\leq N$). See the text for the method of visualization.
(a) $N=100$ and $\varepsilon=0.0018/1.752$. $x_{60n}(i)$'s are plotted for $10<n<310$.
(b) $N=100$ and $\varepsilon=0.0011$. $x_{30n}(i)$'s are plotted for $20<n<320$.
(c) $N=100$ and $\varepsilon=0.0021/1.752$. $x_{27n}(i)$'s are plotted for $0<n<300$.

the patterns in (C), the propagation is not so straight and it moves like Brownian motion, which is expected since the original one-dimensional mapping has a topological chaos. In model (B), the map $f^2(x)$ is monotonically increasing at most parts of x and $x_n(i)$ (without mod) increases monotonically as n for most of the time. Thus, the burst propagation in model (B) is more regular than in (C), which makes the pattern in (B) geometrically more regular.

§ 5. Mechanism

A typical aspect of the patterns in § 4 is that they are formed by the existence of two kinds of propagations, i.e., that of laminar clusters and that of bursts. As an example, we consider the pattern like Fig. 7, which appears with various sizes in Fig. 4. The elementary pattern Fig. 7 is formed by the propagation of laminar regions with speed v_L and that of burst regions with speed v_B. The ratio v_B/v_L is less than one in the patterns in Fig. 4, which goes to zero as ε is decreased. The propagation, of course, does not occur at a constant speed and the speed of the propagation has some fluctuations, though they are very small for model (B), which is the reason why the patterns in Fig. 4 look so regular.

The time series for model (B) for a sequence of lattice points are shown in Fig. 8, which clearly represents the existence of the two kinds of propagation speeds.

What is the mechanism of the existence of two speeds? Roughly speaking, v_L is related with the motion $x_{n+1}=f(x_n)$, while v_B arises from the coupling term $g(x_n(i+1))+g(x_n(i-1))$. Here, we discuss their meanings. The map $f^p(x)$ ($p=2$ for model (B) and 3 for model (C)) has the form

$$f^p(x)-x_i^* \simeq a(x-x_i^*)+\beta(x-x_i^*)^2; \quad a\sim 1$$

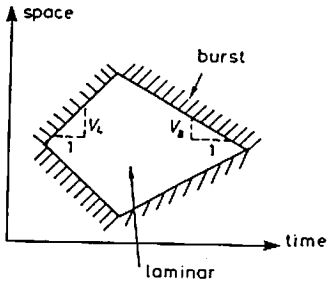

Fig. 7. Schematic representation for the elementary laminar cluster.

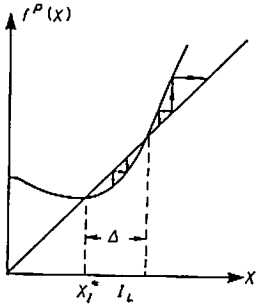

Fig. 9. Schematic representation for $f^p(x)$ near $x=x_i^*$.

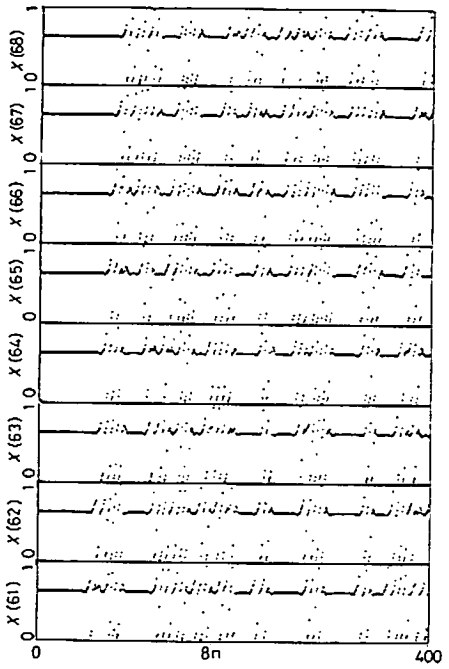

Fig. 8. Time series for model (B) with $\varepsilon=0.024$ for $x_{8n}(61)$, $x_{8n}(62)$, ⋯, and $x_{8n}(68)$ for $0<n<400$. Initial condition is the same as in Fig. 4.

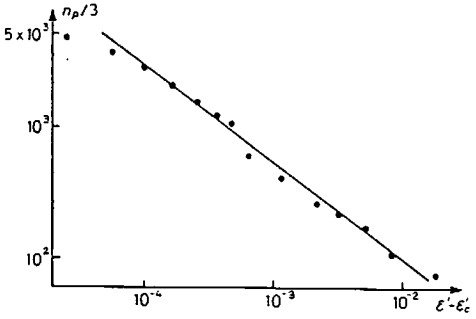

Fig. 10. The propagation time n_p as a function of coupling ε for model (C) with $N=100$ with the initial condition $x(i)=x_1^*$ (for $1<i\leq N/2$) and $x(i)=x_2^*$ (for $N/2<i\leq N$). The notation $\varepsilon'=\varepsilon A$ is used. ε_c' is estimated to be 0.001845. The propagation time is defined as the time step when the bursts from $i=0$ and $i=50$ make the first collision.

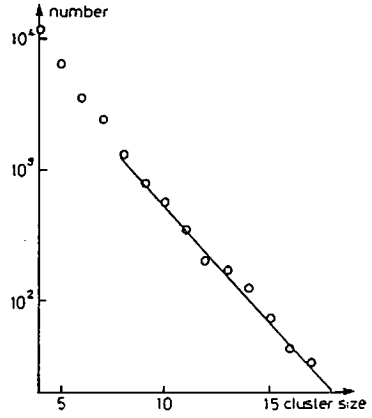

Fig. 11. Cluster distribution for model (B) with $\varepsilon=0.024$ and $N=500$ and the same initial condition as in Fig. 4. $\sum_{i=0}^{3}Q(4n+i)$ is plotted as a function of laminar size n. $Q(n)$ is calculated from the data $x_{2m}(i)$ for $10^4<m<1.5\times10^4$.

near some periodic point x_i^* (see Fig. 9). Assume that the sites $i\leq i_0$ belong to laminar regions I_L (close to x_i^*). The motion of $x(i_0)$ departs from the laminar region only if $x-x_i^*$ exceeds Δ by the effect of $g(x_n(i+1))$. Thus, the propagation of a burst occurs if

$$\varepsilon\sum_{k=1}^{L}\{g(x_k(i_0+1))-x_i^*\}\sim\Delta$$

(in this case the speed of burst propagation v_B is given by L^{-1}). Roughly speaking, $v_B\propto\varepsilon\int_{x\in I_L}(g(x)\rho(x)-x_i^*)dx$ if $g(x_k(i_0+1))$ is replaced by $\int_{x\in I_L}g(x)\rho(x)dx$ where $\rho(x)$ is a distribution function for the coupled map lattice equation. (Of course, this is not correct, since there is a correlation between the motions of nearby lattice points). On the other hand, if $x_k(i_0+1)$ falls onto the region $(x_i^*, x_i^*+\Delta)$ before $\varepsilon\sum_{k=1}^{L}g(x_k(i_0+1))$ happens to exceed Δ, the laminar region propagates up to the region i_0+1. The propagation speed of laminar regions v_L is roughly proportional to $\int_{x\in I_L}\rho(x)dx$.

As ε is decreased, the propagation speed decreases till it vanishes at $\varepsilon\sim\varepsilon_c$. The decrease of v_B is roughly given by $(\varepsilon-\varepsilon_c)^\nu$ with $\nu=(0.6\sim0.9)$. See Fig. 10, for example, for the behavior of the propagation time ($\propto N/v_B$) for model (C), which gives the exponent $\nu\sim0.75$. The exponent ν seems to depend on the models. The accurate calculation of the exponent, however, is rather hard, since the transition does not occur at one point (see Fig. 3) and some data have large deviations from the above power law fit.

Another interesting quantity is the distribution of the size of laminar clusters. In the case of a class-3 cellular automaton,[16] the distribution function of 0-sites decays exponentially if it starts from the disordered configuration, while it shows a power-decay if it starts from a configuration with $x(i)=1$ for $i=i_0$ and 0 otherwise.

Instead of the direct calculation of the distribution function of clusters, the "laminar sequence density" $Q(n)$ is numerically calculated for our model, which is defined as the spatial sequence of exactly n adjacent laminar sites, bordered by sites with bursts. The density $Q(n)$ and the distribution of the laminar cluster $T(n)$ is related by[16]

$$Q(n)\simeq\sum_{i=n}^{\infty}(2T(i)/i)\,.$$

According to the numerical results, the density $Q(n)$ (thus, $T(n)$ also) decays exponentially even if the initial configuration is $x(i)=x_1^*$ $(i\leq i_0)$ and x_2^* $(i>i_0)$ (see Fig. 11). The rate of the decay decreases as ε decreases and at some values of ε close to ε_c, some data show power-decay-like behavior, though, again, the detailed study of the critical phenomena is rather hard.

§ 6. Lyapunov spectra

Numerical results for the calculation of the Lyapunov spectra are shown in this section. Here we choose the initial condition $x(i)=0.2\sin(2\pi i/N)$ and iterated map (C) with $N=50$ by 9000 times after dropping the initial 10000 times of transients. The method of calculation is based on Ref. 20). See Refs. 21) and 22) for the Lyapunov spectra in high dimensional systems. The histograms for the Lyapunov exponents are shown in Fig. 12, where the numbers of the exponents within $[-0.37, -0.32)$, $[-0.32, -0.27)$, ⋯, $[0.38, 0.43)$ are plotted, for $\varepsilon'=0.0019$, 0.00197, 0.0021, 0.0023 and 0.0025 where $\varepsilon'=\varepsilon A=1.752\varepsilon$.

As ε is increased, the number of positive exponents increases. Here we note that the

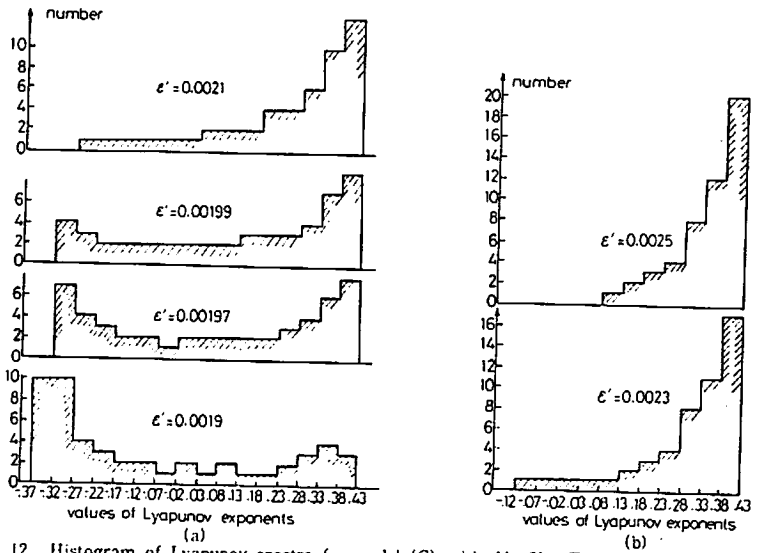

Fig. 12. Histogram of Lyapunov spectra for model (C) with $N=50$. The number of Lyapunov exponents which take the values in the interval $(-0.37+0.05\times j, -0.32+0.05\times j)$ is plotted as a function of j. Initial condition is chosen as $x_0(i)=0.2\sin(2\pi i/N)$. $\varepsilon'=\varepsilon A$. See the text for the method of calculation.

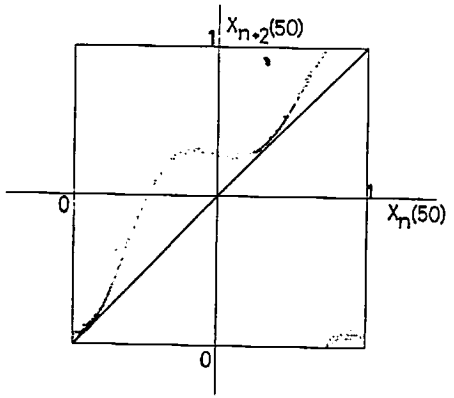

Fig. 13. Plots of $x_{2n+2}(50)$ vs $x_{2n}(50)$ for $1000<n<4000$ for model (B). $N=100$ and $\varepsilon=0.024$. Similar behavior is obtained for model ((C).

histogram has a peak at $\lambda=\beta\sim-0.32$ and $\lambda=\alpha\sim0.40$. As ε is increased, the number at $\lambda\simeq\beta$ decreases and the one at $\lambda\sim\alpha$ increases, while the number at $\lambda\sim0$ remains small. The number $\lambda\sim\beta$ agrees with the exponent for the stable cycle with period three for the one-dimensional map $x_{n+1}=f(x_n)$. Thus, the Lyapunov exponent $\lambda\sim\beta$ corresponds to the laminar part of the motion. On the other hand, the exponent $\lambda\sim\alpha$ is related to the

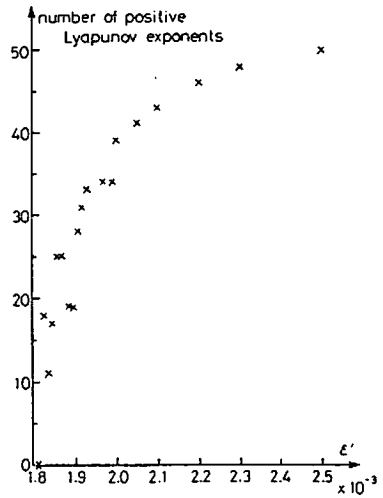

Fig. 14. Number of positive Lyapunov exponents as a function of $\varepsilon'=\varepsilon A$ for model (C) with the initial condition $x(i)=x_1^*$ (for $1<i\leq N/2$) and $x(i)=x_2^*$ (for $N/2<i\leq N$). $N=50$. See the text for the method of calculation.

burst motion in the sense as follows: The data $(x_n(i), x_{n+1}(i))$ from the coupled map lattice equation lie close to a curve $x_{n+1}=F(x_n)$, where $F(x)$ is a function a little bit different from $f(x)$. Of course, the data scatter around $x_{n+1}=F(x_n)$ with some fluctuations. The function $F(x)$ is a sort of a "mean field mapping", in the sense that the average motion of the coupling term $\varepsilon/2\{g(x_n(i+1))+g(x_n(i-1))-2g(x_n(i))\}$ gives a correction $F(x_n(i))-f(x_n(i))$. The mapping $x_{n+1}=F(x_n)$ does not have a stable cycle and it gives a positive Lyapunov exponent about $\lambda\sim\alpha$ (see Fig. 13 for the numerical plot for $F^2(x)$). The fact that many exponents concentrate at $\lambda\sim\alpha$ for large couplings means that the turbulent motion is approximated by the direct product state of the one-dimensional map $x_{n+1}=F(x_n)$, though, of course, some fluctuations around the state exist.

The increase of the number of positive Lyapunov exponents is a process of the development of chaos into higher-dimensional one, though the dimension itself is not calculated here. The number of positive Lyapunov exponents as a function of the bifurcation parameter $\varepsilon'(=\varepsilon A)$ is plotted in Fig. 14, which shows a behavior $(\varepsilon'-\varepsilon_c')^a$ with $a\simeq(1/3\sim1/2)$ where ε_c' is the onset value for the chaotic motion (since the transition does not occur at one point (see Fig. 3), accurate calculation is impossible, but the fine structure in Fig. 3 is seen only in a small range of the parameter and a rough estimate for ε_c is possible).

The dependence of the number of positive exponents on the bifurcation parameter near the onset of chaos is also studied for the cases of the period-doubling and the transition from torus to chaos for the coupled logistic lattice, which shows similar behavior $((\varepsilon-\varepsilon_c)^a;\ a\sim1/2)$ for the increase of the number of positive exponents.

§ 7. Discussion

In the present paper, we have investigated the spatiotemporal intermittency. One characteristic feature is that the laminar clusters form geometrical structures quite analogous to the ones observed in cellular automata. Possible mechanisms are discussed. Another interesting feature is that a picture of "direct product state of chaos" seems to be applicable if the coupling becomes large as is seen in the Lyapunov spectra and in the possibility of a kind of mean field mapping.

Still, the relation between the two "intermittencies" is not clear. It is hoped however, that the present study gives a step for the future study to make a connection between the two notions. Also, some problems are left for future. Especially, (i) detailed studies on

critical phenomena, (ii) propagation of information in connection with the burst propagation, (iii) theory for the propagation of bursts and laminar clusters, (iv) clear explanation for the geometrical structures, (v) Lyapunov vectors and their connection with the burst propagation (vi) construction of a "mean field theory" for the coupled chaos.

Coupled map lattices are very powerful for the study of field theory of chaos and will be used in a variety of fields.

Acknowledgements

The main part of the work was performed before the author left for Los Alamos, though the discussion there was important. The author would like to thank. J. Doyne Farmer,. Gottfried Mayer-Kress, Norman Packard, Stephen Wolfram, Jim Crutchfield. and Jim D. Keeler for useful discussions and comments. He would also like to thank LICEPP (at Univ. of Tokyo) for the facilities of FACOM M190.

References

1) See for recent advances, *Chaos and Statistical Methods*, ed. Y. Kuramoto (Springer, 1984); K. Kaneko, *Collapse of Tori and Genesis of Chaos in Dissipative Systems* (to be published from World Sci. Pub. Co.).
2) L. D. Landau and E. M. Lifshitz, *Fluid Mechanics* (Pergamon Press, 1959).
3) D. Ruelle and F. Takens, Comm. Math. Phys. 20 (1971), 167.
S. Newhouse, D. Ruelle and F. Takens, Comm. Math. Phys. 64 (1978), 35.
4) K. Kaneko, Prog. Theor. Phys. 69 (1983), 403; 71 (1984), 282.
5) K. Kaneko, Prog. Theor. Phys. 72 (1984), 480.
K. Kaneko, *Dynamical Problems in Soliton Systems*, ed. S. Takeno (Springer, 1985), p.272; "Turbulence in Coupled Map Lattices", to appear in Physica D; "Lyapunov Spectra and Vectors in CML", in preparation.
6) J. D. Keeler and J. D. Farmer, private communication.
7) R. Kapral, Phys. Rev. 31A (1985),3868.
8) K. Kaneko, Phys. Lett. 111A (1985), 321.
9) Y. Aizawa, Prog. Theor. Phys. 72 (1984), 662.
10) T. Yamada and H. Fujisaka, Prog. Theor. Phys. 72 (1985), 885.
11) J. Crutchfield and K. Kaneko, in preparation.
12) R. J. Deissler, Phys. Lett. 100A (1984), 451.
13) Y. Aizawa and I. Nishikawa, private communication.
14) Y. Pomeau and P. Manneville, Comm. Math. Phys. 74 (1980), 189.
15) E. A. Novikov and P. W. Stewart, Isv. Akad. Nauk. USSR, Ser. Geophys. 3 (1964), 408.
B. B. Mandelbrot, J. Fluid Mech. 62 (1974), 331.
U. Frisch, P. L. Sulem and M. Nelkin, J. Fluid Mech. 87 (1978), 719.
16) S. Wolfram, Rev. Mod. Phys. 55 (1983), 601.
16) S. Takesue and K. Kaneko, Prog. Theor. Phys. 71 (1984), 35.
18) C. Grebogi, E. Ott and J. A. Yorke, Physica 7D (1983), 181.
19) D. K. Campbell, J. F. Schonfeld and C. A. Wingate, Physica 9D (1983), 1.
20) I. Shimada and T. Nagashima, Prog. Theor. Phys. 61 (1979), 1605.
21) J. D. Farmer, Physica 4D (1982), 366.
22) Y. Pomeau, A. Pumir and P. Pelce, J. Stat. Phys. 37 (1984), 39.